


# Effect of nano bentonite on direct yellow 50 dye removal; Adsorption isotherm, kinetic analysis, and thermodynamic behavior

Progress in Reaction Kinetics and Mechanism  
Volume 47: 1–23  
© The Author(s) 2022  
Article reuse guidelines:  
[sagepub.com/journals-permissions](https://sagepub.com/journals-permissions)  
DOI: 10.1177/14686783221090377  
[journals.sagepub.com/home/prk](https://journals.sagepub.com/home/prk)  


Ahmed S. Mahmoud, Ph.D.

## Abstract

Developing countries suffering from the toxicity of different industrial effluents especially dyes. This study successfully prepared and characterized nano-bentonite for anionic dye removal (DY 50). The prepared nanoparticles were characterized by X-Ray Diffraction (XRD), X-ray Fluorescence (XRF), Scanning Electron Microscope (SEM), EDAX analysis, FT-IR, and TGA and the obtained results indicated the formation of nanoparticles with an average size of 15 nm. The effect of different operating conditions was studied using different pH, dose, contact time, temperature, and initial DY 50 concentrations. The obtained results indicated that nano bentonite was able to adsorb about 78.3 and 100% for initial concentrations of  $100 \pm 8.1$  and  $20 \pm 1.62$  mg/L, respectively. The optimum removal conditions were observed at acidic media (pH 3) using sorbent material dosage 1 g/L for 45 min and 30°C. The adsorption isotherm, kinetic analysis, and thermodynamic behavior were studied by using linear equation form, and the adjusted  $R^2$  was compared to detect the preferred models. The adsorption isotherm indicated that heterogeneous, as well as multilayer adsorption, plays an important role in the removal of dye. Kinetic studies indicated the chemisorption interaction between sorbed and adsorbed molecules. Thermodynamic behavior indicated the reaction is exothermic with  $\Delta H$  equal to  $-5.24$  KJ/mol and  $\Delta S$  equal  $-74.2$  J/K.mol. Finally, this study strongly recommended using nano bentonite for DY 50 removal from an aqueous solution. The RSM relations show significant relations in all removal models with  $p$ -value  $< 0.001$ . The ANN results indicated that the most effective operating conditions are the effect of nano bentonite dose followed by the pH effect.

Scientific Research Development Unit, Egyptian Russian University (ERU), Badr, Egypt

## Corresponding author:

Ahmed S Mahmoud, Scientific Research Development Unit, Egyptian Russian University (ERU), Badr, Egypt .  
Email: [ahmeds197@gmail.com](mailto:ahmeds197@gmail.com); [Ahmed-said@eru.edu.eg](mailto:Ahmed-said@eru.edu.eg)



Creative Commons Non Commercial CC BY-NC: This article is distributed under the terms of the Creative Commons Attribution-NonCommercial 4.0 License (<https://creativecommons.org/licenses/by-nc/4.0/>) which permits non-commercial use, reproduction and distribution of the work without further permission provided the original work is attributed as specified on the SAGE and Open Access pages (<https://us.sagepub.com/en-us/nam/open-access-at-sage>).

## Keywords

Nano-bentonite, adsorption isotherm, regression analysis, direct yellow 50, Climate Changes

## Introduction

Water is the most important polar solvent all over the world.<sup>1</sup> So, it can carry out a wide range of inorganic and organic pollutants. The reuse of wastewater is the most important solution to overcome water scarcity problems.<sup>2</sup> Soluble organic contaminants are the most hazardous pollutants that all countries faced and have difficulties getting rid of these contaminants in economic and fast ways.<sup>3,4</sup> Different types of organic contaminants may affect water quality such as color, pesticides, carbon, nitrogen, and sulfur pollutants.<sup>5-8</sup> Color contaminants are one of the most common water and wastewater contaminants. The presence of color in water and wastewater indicated the presence of a high number of organic carbons in water or wastewater.<sup>5</sup>

Colors may be present in raw water as the colloidal form produced from the presence of some particles such as lignins, humic acids, tannins, textiles, acids such as fulvic acids, and other similar compounds.<sup>9,10</sup> Industrial projects affect watercolor and cause color pollution such as the yellow color of fermented washing, dark color of bottling plant, and brown color of spent wash.<sup>11</sup> The presence of harmful strains of cyanobacterial algal that formed cyanotoxins also affects water quality by creating unwanted colors.<sup>12</sup> There are different contaminated sites by color all over the world and the most popular contaminated site in China is the yellow color which comes from chromium slag produced by Lvliang Chemical Industry.<sup>13</sup> Also, Egypt has different color polluted areas such as red color in temporary Borg El-Arab industrial drain area, Alexandria and green color in the industrial Badr city, Egypt. The color of industrial wastewater is often a significant characteristic, especially in the textile, paper, food, and clothing industries.<sup>14</sup> The coloring of industrial wastewater is produced by ions of chrome, copper, nickel, and iron salts. Metal ions can release green and yellow colors in case of the oxidation state of chrome, blue and green in case of copper and nickel, and yellow and brown in different oxidation states of iron. Also, the soluble anionic or/and cationic dyes and insoluble dyes used in the textile, paper, and leather industries produce very intense colors that linger even after repeated dilution.<sup>15-17</sup> The coloring of wastewater can also be caused by suspensions of colloidal and non-soluble substances and lubricants.<sup>18,19</sup> In other cases, the color may develop in the water because of the effect of mixing different types of wastes.<sup>20-22</sup> The release of these pollutants without proper treatment poses a significant threat to both the environment and public health. Thus, their treatment becomes inevitable.<sup>23,24</sup> Direct yellow 50 is one of these contaminants that may affect the quality of water.<sup>25</sup>

Different technologies were used to remove organic contaminants.<sup>8</sup> The coagulation, degradation, and adsorption techniques are the most common treatment processes used for organic contaminants removal.<sup>26-29</sup> Chemical coagulation, electrocoagulation, biodegradation, and filtration are also used for moderate organic and color removal.<sup>28,30-32</sup> Wastewater physicochemical treatment processes are the most visible in the primary treatment process in a wastewater treatment plant.<sup>33,34</sup> Although the primary treatment processes in different wastewater treatment plants are the commonest, they include several types of other physicochemical processing that may be classified into a small number of units during the operating process.<sup>35,36</sup> Physicochemical processes in the primary treatment of industrial wastewater are designed to remove particulates and other common materials from the effluent before the secondary treatment processes.<sup>37,38</sup> The separated solids are used in both aerobic and anaerobic digesters.<sup>39,40</sup> In the primary treatment, exclusive physicochemical processes are employed to isolate suspended solids, oil, and greases from wastewater.<sup>41,42</sup>

The primary treatment of wastewater usually includes screening, flocculation, flotation, sedimentation, and granular sand filtration.<sup>43,44</sup> In a conventional wastewater treatment plant, wastewater is regularly taken in a tank for some hours to allow settling to the bottom and the greases to float to the top.<sup>45-47</sup> The solids picked from the bottom and floated oil in the top were received, and the purified raw wastewater continues to the next step of the treatment.<sup>48,49</sup> The exact progression of unit operations is mainly dependent on the wastewater characteristics, objectives of treatment, and local environmental laws and regulations.<sup>50-52</sup> Recently, nanotechnologies are commonly been used for organic removal from wastewater.<sup>1,53,54</sup>

Nano bentonite has a strong ability to adsorb a wide range of water and wastewater contaminants due to high surface and reactivity.<sup>55</sup> Joshi et al. (2004) studied color removal from textile effluent using different techniques and indicated the ability of bentonite to adsorb basic dyes.<sup>56</sup> Mukhopadhyay et al. (2019) studied bicarbonate and nitrite removal from wastewater using nanoparticles (Iron Oxide and bentonite) and the obtained results indicated that Fe-exchanged nano-bentonite can adsorb 29.33 mg/g after 120 min with significantly less than 0.05.<sup>57</sup> Jana et al. (2019) studied the efficient removal of cationic organic dye using nanocomposite incorporated bentonite.<sup>58</sup> Chinoune et al. (2016) studied reactive dyes removal from aqueous solution using dirty bentonite and the obtained results indicated that the B-Mg(OH)<sub>2</sub> has strong ability to adsorb a wide range of dye concentration reached ~50 mg/g at acidic media after 3h from contact time.<sup>59</sup>

This study attempts to examine the removal of DY 50 from aqueous solutions using nano bentonite. The prepared nano bentonite was well characteristic for DY 50 removal. The effect of different operating conditions was conducted to optimize the effective conditions. Finally, the adsorption isotherms, kinetic studies, and thermodynamic behavior were designed to describe the reaction mechanism, equilibrium state, and spontaneity of the reaction. Also, the RSM relation was obtained using linear regression analysis to detect the significance of the adsorption process and produce the general DY 50 removal % equation not only for optimum conditions but also for all experimental results. Finally, the artificial intelligence neural network was conducted to predict the importance of each operating parameter and to predict the relations between calculated and experimental removal efficiency.

## Materials and methods

### *Chemical and reagents*

The following chemicals were used in the current study: Pure Egyptian Bentonite powder, DY 50 powder (C<sub>35</sub>H<sub>24</sub>N<sub>6</sub>Na<sub>4</sub>O<sub>13</sub>S<sub>4</sub>, 98.5%, Pub-chem), Sodium hydroxide (NaOH, 99% pure, Oxford Co.), and Sulfuric Acid (H<sub>2</sub>SO<sub>4</sub>, 98%, Honeywell - Fisher Co.).

### *Preparations*

*Preparation of nano bentonite.* Nano bentonite was prepared by using flotation and sedimentation techniques. The Pure Egyptian Bentonite Raw was softened and dried at 105°C for 2 hours, cooling the bentonite powder was well mixed with deionized water by a ratio of 1:1, shaking at 300 rpm for 3 min, soaked for 24 h, shaking again at 100 rpm for 30 min, and settling for 2h. The floated nanoparticles were filtrated by using Whatman filter paper No. 1 (150 mm), dried at 105°C, and stored in a glass bottle. The structure of the DY 50 powder sample is presented in [Supplementary Fig. 1](#).

*Preparation of standard DY 50 dye aqueous solution.* About 1.02 g of pure DY 50 powder was dissolved in 1L of deionized water to prepare 1000 ppm from standard DY 50 solution. The prepared standard solution was scanned by a Uv-Vis scanning spectrum with a range between 190 and 1000 nm for 20 min to optimize the suitable wavelength of the experiment to build the calibration curve. Three identified peaks were observed and the maximum peak was observed at  $\lambda = 412$  nm after scanning was completed. Different dye concentrations were prepared to build the calibration curve, quality control, and uncertainty measurements. The selected concentrations for the calibration curve were  $1 \pm 0.8$ ,  $3 \pm 0.24$ ,  $5 \pm 0.41$ ,  $7 \pm 0.81$ ,  $10 \pm 0.81$ ,  $15 \pm 1.21$ ,  $20 \pm 1.62$ , and  $30 \pm 2.43$  mg/L.<sup>60</sup>

### *Point of zero charge of nano-bentonite*

About 7.455 g of KCL was dissolved in 1 L of deionized water to prepare 0.1 m from KCl solution. Exactly 200 mL from the prepared DY 50 solution was added directly into a 1L Erlenmeyer flask and the pH values were adjusted to 2, 3, 4, 5, 6, 7, 8, 9, 10, 11, and 12 by using 1 N H<sub>2</sub>SO<sub>4</sub> and 1 N NaOH (pH<sub>i</sub>). About 0.1 g of dried nano bentonite was added separately into the adjusted flasks and left 24 h at room temperature. The final pH was measured by using AD 8000-Adwa pH meter (pH<sub>f</sub>). Averaged values of pH changes after nano bentonite modifications were obtained from 3 measurements and all standard deviation values were within  $\pm 0.05$ . The point of zero charges of nano bentonite was calculated by plotting the relation between  $\Delta$ pH values (final pH – initial pH<sub>i</sub>) and initial pH values (pH<sub>i</sub>).<sup>61</sup>

### *Uncertainty measurements*

Two main steps were optimized for uncertainty calculations. First, the uncertainty of standard DY 50 was calculated by calculating the relative uncertainty of all expected errors. The square root of relative uncertainty of salt purity, balance, pipette, and the volumetric flask was calculated to estimate the combined uncertainty. The expanded uncertainty was calculated to cover 95% of the results. The final uncertainty of 1000 mg/L of DY 50 was  $\pm 17.809$  mg/L. Second, the uncertainty calculations of calibration curve combined with standard DY 50 uncertainty, Uv-Vis spectrophotometer uncertainty below and above abs. 1.000. The final relative uncertainty was 8.104%.

### *Characterization*

The prepared nano bentonite powder sample was investigated using x-ray diffraction patterns (XRD), XRF, SEM, EDAX analysis, and particle size distribution. A Philips XRG 3100 diffractometer manufactured by Philips Electronics Company, the Netherlands, was utilized for performing XRD analysis. It uses copper K-alpha radiation and a graphite monochromator to generate x-rays with a wavelength of 1.5418 Å. The X-Ray current and voltage are 40 kV and 40 mA, respectively. XRF analysis was conducted by using Axios Max DY 2063, PANalytical. The XRD and XRF analyses were conducted at certified iso 17025 material institute, Housing and Building National Research Center, Egypt. The prepared nano bentonite powder sample was placed in a stainless steel holder and scanned for a range from 5° to 80° with a rate of 0.0167°/sec due to the absence of any peak before 35°. <sup>2,4</sup> A Philips Quanta 250 FEG manufactured by Philips Electronics Company, USA, was utilized for performing the SEM analysis. The SEM instrument operates at a magnification of 120,000x and a voltage of 20 KV. FTIR was analyzed before DY 50 treatments by nano bentonite using FT/IR-6100typeA, S/N A009061020 with a standard light source and TGS

detector. The FTIR resolution was  $8 \text{ cm}^{-1}$  and the 10000 Hz filter. The SEM and FTIR instruments were placed at the National Research Center (NRC). Particle size distribution analysis was conducted for dried samples by using Microvision (particle size measurement) located at CID Company for pharmaceutical industries, Egypt, using  $\mu$  u-tech production, and model VGA-410 France.

### Experimental setup

In the first experiment, the adsorption of DY 50 was studied by batch techniques using a one-factor method. The operating parameters and their normal ranges of variation were identified based on the literature review. Table 1 summarizes the conducted batch experiments at different operating parameters (pH, dose, contact time, concentration, and temperature). A known weight of adsorbent 1 g/L was equilibrated with 1000 mL of an anionic DY 50 solution of known concentrations (20–100 mg/L) in 1000 mL of Erlenmeyer flasks and shaken for a known. After equilibration, the suspension of the adsorbent was separated using Whatman filter paper No. 1, and the remaining concentrations were measured using a T 70+ Uv-Vis spectrophotometer at  $\lambda = 412 \text{ nm}$  and verified by using Apcl spectrophotometer 101 using filter 410 nm. The selected wavelength shows agreement with previous studies.<sup>62</sup> The percentage of removal efficiency was calculated using equation (1). The amount of sorbed dye was calculated using equation (2), and all experiments were performed in triplicate<sup>63,64</sup>

$$\text{Sorption (\%)} = \left( \frac{C_0 - C_e}{C_0} \right) \times 100 \quad (1)$$

where  $C_o$  is the initial DY 50 concentration (mg/L) and  $C_e$  is the equilibrium concentration in solution (mg/L)

$$Q_e(\text{mg/g}) = \frac{(C_0 - C_e)V}{m} \quad (2)$$

where  $q_e$  is the equilibrium adsorption capacity (mg/g), V is the volume of aqueous solution (L), and m is the dry weight of the adsorbent (mg).

Through the adsorption experimentations, the amount of the DY 50 filtered and removed at multiple interludes was evaluated using equation (2)

$$Q_t = \frac{(C_0 - C_t)V}{W} \quad (3)$$

**Table 1.** Batch experiments at different operating parameters.

Effect	Dose (g)	Contact time (min)	pH	Concentration (mg/L)	Temperature ( $^{\circ}\text{C}$ )
<b>Effect of pH</b>	1	45	2 - 10	40	30
<b>Effect of adsorbent dose</b>	0.2–1.8	45	3	40	30
<b>Effect of contact time</b>	1	10–360	3	40	30
<b>Effect of stirring rate</b>	1	45	3	40	30
<b>Effect of concentration</b>	1	45	3	20–100	30
<b>Effect of temperature</b>	1	45	3	40	20–70

where  $C_t$  represents DY 50 concentration in liquid (mg/L) at different periods “t”.

### *Isotherm studies*

Nonlinear two and three isotherm models were utilized to explain the adsorption behavior of anionic dyes represented in DY 50 dye from an aqueous solution onto the solid phase of nano bentonite at equilibrium environments at a constant temperature. These models include two-parameter isotherm models as Freundlich, Langmuir, and Jovanovich, and three-parameter isotherm models as Redlich–Peterson, Hill, Sips, Khan, Toth, and Koble–Corrigan. The nonlinear equation for both two parameters and three parameters isotherm model and its description are presented in [Supplementary Table S1](#).<sup>27,65,66</sup>

### *Kinetic studies*

The kinetics adsorption of anionic dyes represented in DY 50 onto nano bentonite was calculated using nonlinear kinetic models. These models include pseudo-first-order (PFO), pseudo-second-order (PSO), Avrami, Elovich, and Intraparticle models. The nonlinear equations for all kinetic models are presented in [Supplementary Table S2](#).

### *Validation of adsorption isotherms and kinetics*

Five design error functions were calculated to explain the better fit of kinetic and isotherm nonlinear equations to evaluate the model results. These error equations include Chi errors, Marquardt’s percent standard deviation (MPSD), a Composite Fractional Error Function (HYBRD), the Sum of the Squares of the Errors (ERRSQ), the Sum of the Absolute Errors (EABS), and Average Relative Error (ARE).<sup>51</sup> The error functions are presented in [Supplementary Table S3](#), and the lowest error type was used for preferred model estimation.

### *Thermodynamic behavior*

Different thermodynamic parameters were calculated to describe thermodynamic behaviors after interaction between sorbed and adsorbed molecules as Gibbs free energy ( $\Delta G$ ), enthalpy ( $\Delta H$ ), and standard entropy ( $\Delta S$ ). The thermodynamic results can be calculated by using equations (4–6)

$$\Delta G^0 = \Delta H^0 - T\Delta S^0 \quad (4)$$

$$\Delta G^0 = -RT\ln K_d \quad (5)$$

$$\ln(K_d) = \frac{\Delta S^0}{R} - \frac{\Delta H^0}{R} \times \frac{1}{T}, R(8.314 \text{ J/mol K}) \quad (6)$$

if  $\Delta H < 0$ , the reaction tends to be exothermic, if  $\Delta S < 0$  that means a decrease in disorder between sorbed and adsorbed molecules, and if  $\Delta G < 0$  indicates the interaction between sorbed and adsorbed molecules has spontaneous nature.<sup>67,68</sup>

### Neural network structure

An artificial intelligence networks technique was a familiar technique to estimate the removal efficiency, the importance of each operating parameter, and predict the relations between predicted and measured values. The ANN model combined the input covariable (pH, dose, contact time, temperature, and DY 50 concentrations) with hidden layers (weight and bias) and the final output removal layer. The estimated ANN structure for DY 50 removal using nano bentonite was expressed as 5 – 3 – 1 as shown in Figure 1. The network name is “Multilayer perceptron (MLP),” this function used a feedforward backpropagation style and can have multiple hidden layers. It is one of the most regularly used ANN techniques before designing a full-scale model.<sup>1,66</sup>

### Response surface methodology

A pure linear regression equation was employed to determine the relationship between operating conditions (pH, contact time, adsorbent dose, temperature, and concentration) on anionic DY 50 removal efficiency (Equation (7)). All significant values were used to predict the parameters of the model.<sup>57</sup> The coefficient of determination statistical measure ( $r^2$  value) and the  $p$ -value of the predicted model were used to evaluate the accuracy of the model. Finally, the  $t$ -test results were used to assess the final statistical significance

$$Y = \beta_0 + \beta_1x_1 + \beta_2x_2 + \beta_3x_3 + \beta_4x_4 + \beta_5x_5 \tag{7}$$

where Y is the predicted response of DY 50 removal efficiency (%);  $x_1$  is the pH (2 – 10);  $x_2$  is the adsorbent dose (0.2–1.8 g/L);  $x_3$  is the temperature (20–70 rpm);  $x_4$  is the contact time (10–360vmin);  $x_5$  is the concentration (20–100 mg/L);  $\beta_0$  is the model intercept; and  $\beta_1, \beta_2, \beta_3, \beta_4,$  and  $\beta_5$  are the linear coefficients of  $x_1, x_2, x_3, x_4,$  and  $x_5,$  respectively.<sup>6,29,30</sup>

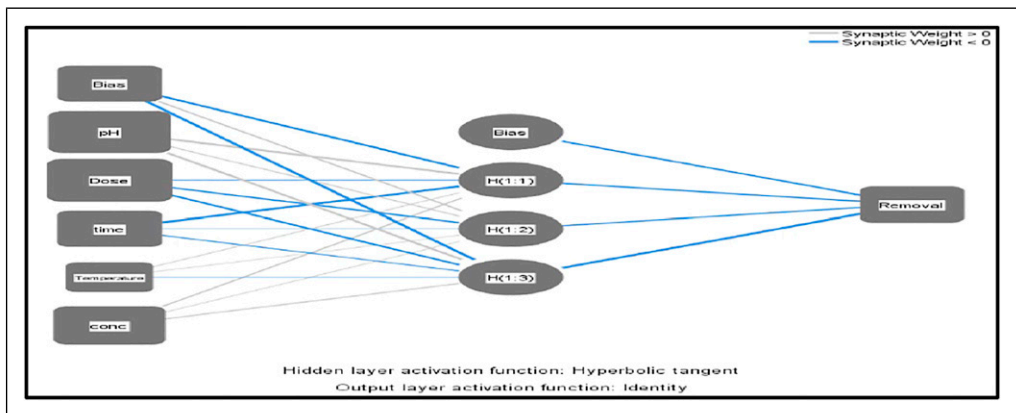


Figure 1. ANN of 5 – 3 – 1 structure used for the prediction of Cr removal efficiency.

## Results and discussion

### Characterization

Nano bentonite was characterized by using X-Ray diffraction (XRD), Scanning Electron Microscope (SEM), EDAX analysis, and FT-IR. The obtained results indicated the formation of nano bentonite and showing agreement with the previous studies.<sup>69–71</sup>

**XRD and XRF characterization.** Figure 2 shows XRD analysis of nano bentonite indicated that about 87% of the nano-bentonite structure contains Si, Al, and Fe. The presence of alfa iron (Fe) was identified by two identified peaks at  $2\theta$  equal  $44.65^\circ$ ,  $64.98^\circ$ , and  $82.53^\circ$  that fit well with the body-centered structure of iron, presence of aluminum (Al) was identified by three identified peaks at  $2\theta$  equals  $38.57^\circ$ ,  $65.27^\circ$ , and  $78.68^\circ$ , and presence of silicon (Si) was identified by one main peak at  $2\theta$   $28.441^\circ$  with (111) coordination. Also, the XRD pattern indicated the formation of small quantities of calcium (Ca), chloride (Cl), titanium (Ti), potassium (K), and manganese (Mn).

Table 2 describes the XRF analysis of nano bentonite showing agreement with XRD results indicating the presence of  $\text{SiO}_2$ ,  $\text{Al}_2\text{O}_3$ , and  $\text{Fe}_2\text{O}_3$  as the main components.

**SEM and EDAX characterization.** Scanning Electron Microscope (SEM) with EDAX analysis was tested for nano-bentonite samples. Figure 3(a) shows the formation of nano bentonite with equal size ranged between 10 and 22 nm. Figure 3(b) shows the EDAX element determination map indicating the domination of Si, Al, and Fe in the nano-bentonite sample. Also, the results indicated the presence of oxygen, silicon, iron, aluminum, calcium, and magnesium in the bentonite sample showing agreement with the XRD, XRF results, and previous studies.

**Particle size distribution and point of zero charges (PZC).** Particle size distribution was tested for nano-bentonite samples from 0 to  $30\ \mu\text{m}$  by a rate of  $0.02\ \mu\text{m}$  as shown in Figure 4(a). The obtained results indicated that 94% of nano-bentonite powder was 50 nm. The point of zero charges (pzc) values for nano bentonite was about 7.85 as shown in Figure 4(b). Khatamian et al., 2019 determined the  $\text{pH}_{\text{PZC}}$  of  $\text{Fe}_3\text{O}_4$ / bentonite nanocomposite using the same technique and the obtained results

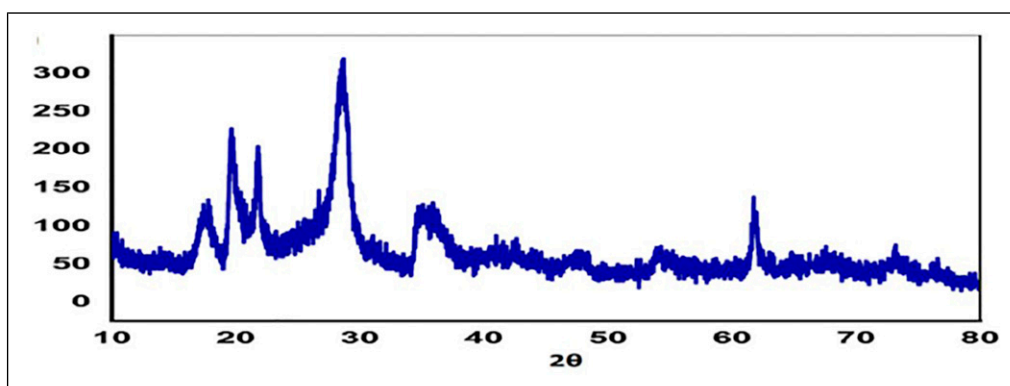
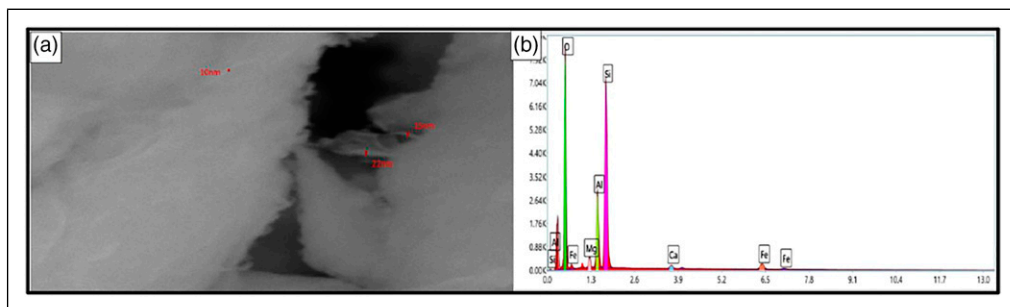
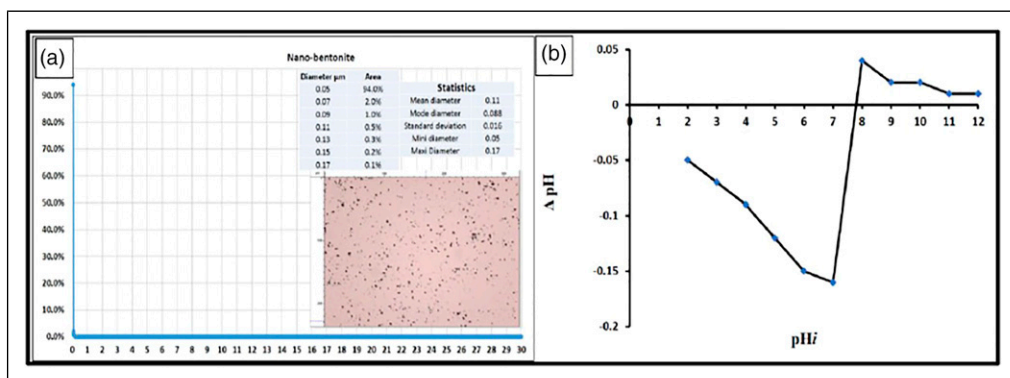


Figure 2. X-Ray diffraction of dried nano-bentonite sample.



**Table 2.** XRF results of the prepared nano bentonite.

Element	SiO <sub>2</sub>	Al <sub>2</sub> O <sub>3</sub>	Fe <sub>2</sub> O <sub>3</sub>	CaO	TiO <sub>2</sub>	K <sub>2</sub> O	MgO	Na <sub>2</sub> O
At%	63.7	19.8	8.85	1.93	1.22	2.05	1.64	0.81

**Figure 3.** (a) Nano bentonite with scale 1 μm, and (b) EDAX element determination map.**Figure 4.** (a) Particle size distribution of the nano-bentonite sample and (b) point of zero charge estimation.

indicated the  $pH_{PZC}$  was 7.3.<sup>72</sup> Dehghani et al., 2020 determined the  $pH_{PZC}$  of modified zero-valent iron and the obtained results indicated that PZC was 8.2.<sup>73</sup> Naghizadeh et al., 2017 determined the  $pH_{PZC}$  of bentonite and the obtained results indicated that the PZC was 7.4.<sup>74</sup> At the point of zero charges, the nanopowder tends to be zero, and below this point can help to chemically adsorb anionic dyes from aqueous solutions.

**FT-IR and TGA Characterization.** Figure 5(a) shows the FT-IR results of the prepared samples showing O-H vibration band between 3600 and 3300  $cm^{-1}$ , Si-O stretching vibration band at 1035  $cm^{-1}$ , Si-O bending vibration band between 526 and 471  $cm^{-1}$ , and Al-O-Si stretching vibration band at 800  $cm^{-1}$ . The obtained FT-IR results agree with the previous nano bentonite characterization studies.<sup>70,75</sup> Figure 5(b) shows the TGA results of the prepared nano-bentonite

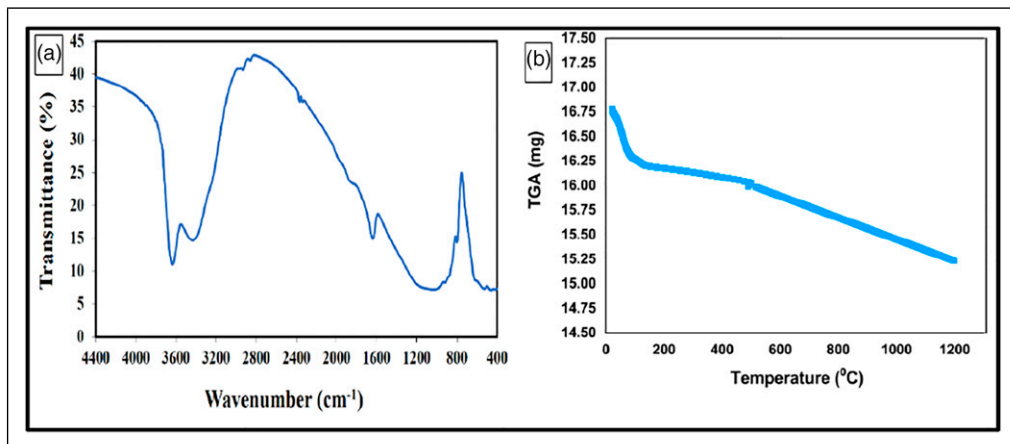


**Figure 5.** (a) FT-IR of nano-bentonite sample, and (b) TGA analysis of nano-bentonite sample.

sample at a temperature between 20 and 1200°C and the obtained results showing weight loss between 16.78°C and 15.23°C with loss percent 2% at 600°C and 9.2% at 1200°C.<sup>70</sup>

### Effect of operating conditions

**Effect of pH.** The effect of pH was studied at different pH ranges from pH 2 to pH 10. The results indicated that the effective pH at acidic pH 3 and the removal percentage was 94.6. At pH 2, the removal percentage was 89.9%. At pH 4, 5, 6, 7, 8, 9, and 10, the removal percentages were 92.3, 85.7, 82.5, 80.1, 77.1, 75.6, and 72.3%, respectively, as shown in Figure 6(a). Joshi et al. (2004) studied a review for decoloring from the textile effluents and mentioned that the optimum pH was 3 after using Fenton's reagent, pH 3.5 better than 7 for chlorination technique, and pH 3–4 after using chitin and chitosan showing agreement with the obtained results.<sup>56</sup> Jabli et al., 2017 studied DY 50 adsorption by the modified waste of palm date fruits with dimethyl diallyl ammonium chloride and diallylamin co-polymer and the obtained results indicated that maximum DY 50 removal occurred at pH 4. At acidic pH, the amount of H<sup>+</sup> increased in the solution and the surface of sorbent material tends to be positively charged and can be able to adsorb the negatively charged dye (-SO<sub>3</sub><sup>-</sup>) by chemisorption process showing agreement with the kinetic studies.<sup>76</sup>

**Effect of dose.** The effect of nano bentonite dose was studied using different doses, namely, 0.2, 0.4, 0.6, 0.8, 1.0, 1.2, 1.4, 1.6, and 1.8 g/L and the removal percentages were 81.2, 84.3, 88.1, 91.5, 94.6, 96.8, 98.6, 99.6, and 100%, respectively, as shown in Figure 6(b). As the dose increases, the vacant sites increase and the removal percentages increase, and the minimum effective dose was 1 g/L. Mahmoud et al. (2019) studied soluble organic matter removal using nano Zero Valent Aluminum (nZVAL) and the obtained results indicated that the removal percentages increased as dose increase and the minimum effective dose was 0.6 g/L with efficient removal percentages of 73%.<sup>1</sup> Different studies were conducted for DY 50 adsorption using different materials such as Organoclay adsorbent, Sugarcane bagasse biomass, and Sugarcane bagasse biomass

treated with polyethyleneimine and the maximum uptake was observed at pH 3, 2, and 2, respectively.<sup>67,77,78</sup>

**Effect of contact time.** The effect of contact time was studied at different times (10, 20, 30, 45, 60, 120, 180, 240, and 360 min). The obtained results indicated that the removal efficiency increased with time and the minimum effective time was 45 min with a removal percentage of 94.6% as shown in Figure 6(c). In the beginning, the removal percentages exceeded 90% due to the high surface area and reactivity of nano bentonite, and the removal percentages were 91.2, 91.9, 92.4, 94.6, 95.4, 96.5, 97.3, 98.2, and 99.1 at times 10, 20, 30, 45, 60, 120, 180, 240, and 360 min, respectively. Enaas 2015 studied DY 50 removal using Natural Clay and Organoclay and the obtained results indicated that the maximum time was 40 min after using bentonite and modified bentonite as sorbent materials.<sup>77</sup>

**Effect of temperature.** The textile industry produces high temperature wastewater which may affect chemical and biological treatment. The effect of temperature was studied at different temperatures, namely, 20, 30, 40, 50, 60, and 70°C and the removal percentages were 94.5, 94.6, 94.4, 93.9, 93.7, and 92.5%, respectively. The obtained results indicated that the most effective temperature was 30°C.

**Effect of concentration.** The effect of initial concentration was studied at different DY 50 concentrations. The removal percentages were 100, 94.6, 89.5, 83.8 and 78.3% for initial concentrations 20, 40, 60, 80 and 100 mg/L, respectively, as shown in Supplementary Figure 2(a). The removal percentages decreased as the initial concentration increased and the selected most suitable concentration for the selected nano bentonite dose was 40 mg/L as shown in Supplementary Figure 2(b).

**Adsorption isotherm.** The adsorption isotherms were calculated by applying two and three nonlinear equations of Langmuir, Freundlich, Redlich-Peterson, Sips, Hill, Khan, Koble–Corrigan, Toth, and Javanovic models. The results indicated that nano bentonite obeys both Freundlich and Koble–Corrigan models (with the same lowest error sum of 0.1728 as represented in Table 3). These results also suggested that the surface of nano bentonite for adsorption of DY 50 dye is heterogeneous, as well as multilayer adsorption plays an important role in the removal of dye. The value of  $n$  is greater than unity ( $n = 4.24$ ), indicating the favorable adsorption of DY 50 anions onto nano bentonite. Koble–Corrigan model combines Langmuir and Freundlich's adsorption isotherm models along with the adsorption isotherm for pure dye material. This indicated that the surface of bentonite for adsorption of DY 50 combined both homogeneous and heterogeneous uptake. Meanwhile, comparing the MPSD of the Freundlich and Langmuir models, we could suggest that heterogeneous uptake was the major mechanism of the adsorption process.

By applying the obtained model constants, the calculated  $Q_e$  can be calculated. Table 4 describes the obtained experimental and calculated  $Q_e$  (mg/g) after using nano bentonite for anionic DY 50 removal. Figure 7(a) describes the relation between  $C_e$  and  $Q_e$  for all adsorption isotherm models including experimental  $Q_e$ .

**Kinetic Studies.** The kinetic studies were carried out by applying the Pseudo First Order (P.F.O), Pseudo Second Order (P.S.O), Elovich, Avrami, and Intraparticle kinetic models. The results indicated that the Avrami model is the best model for the adsorption mechanism followed by

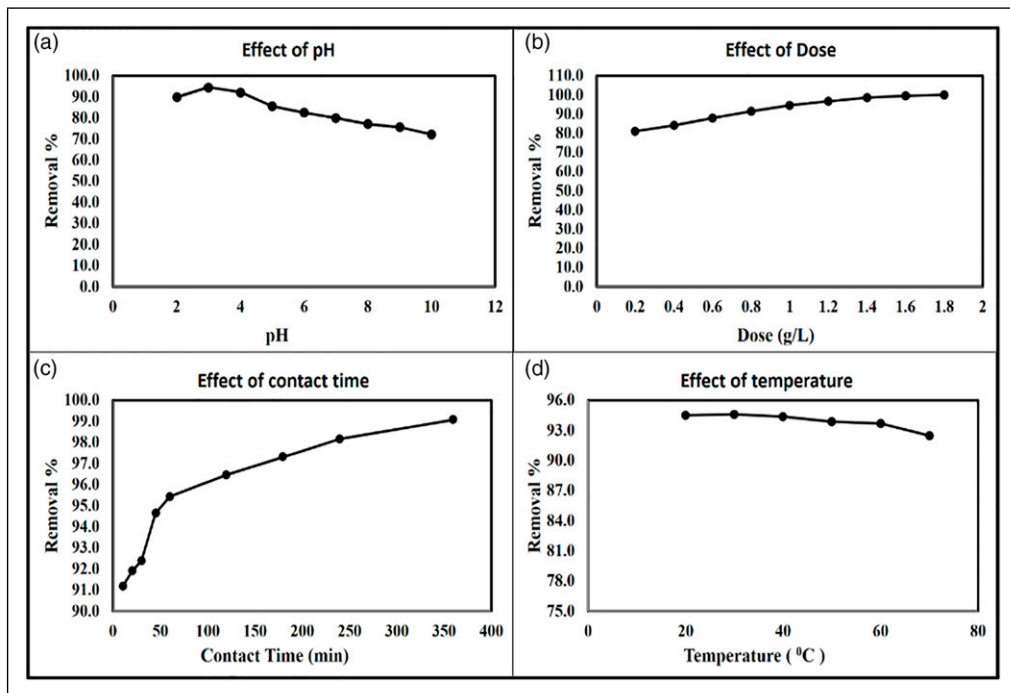


**Figure 6.** (a) Effect of pH, (b) effect of dose, (c) effect of contact time, and (d) effect of temperature.

P.S.O with the minimum MPSD errors of 0.00146 and 0.00222, respectively. According to the Avrami model, the chemical reaction is a significant feature that controls the kinetic process.<sup>79</sup> P.S.O kinetic mechanism indicated that the desorption of DY 50 onto nano bentonite depends on both concentration and dose, and the adsorption mechanism is chemically rate controlling. Additionally, it indicated that the electrons are covalently exchanged or shared between sorbate and sorbent, meaning that the reaction is chemisorptions.<sup>27</sup> According to the Avrami and P.S.O kinetic models, the maximum uptakes were 89.8 and 89.38 mg/g, respectively. Table 5 describes the estimated constants after using nonlinear kinetic relation calculations.

Figure 7(b) describes the relation between experimental and calculated  $Q_t$  (mg/g) and time (min), indicating the small deviations between experimental and calculated  $Q_t$  especially in the case of the Avrami model.

**Thermodynamic analysis.** Thermodynamic studies indicated that the reaction is exothermic as shown in Table 6 and Supplementary Figure (3). Different studies were conducted for DY 50 removal and the obtained results indicated that the reaction has spontaneously occurred with decreases in disorder between sorbed and adsorbed molecules showing agreement with the obtained results.<sup>67,80,81</sup>

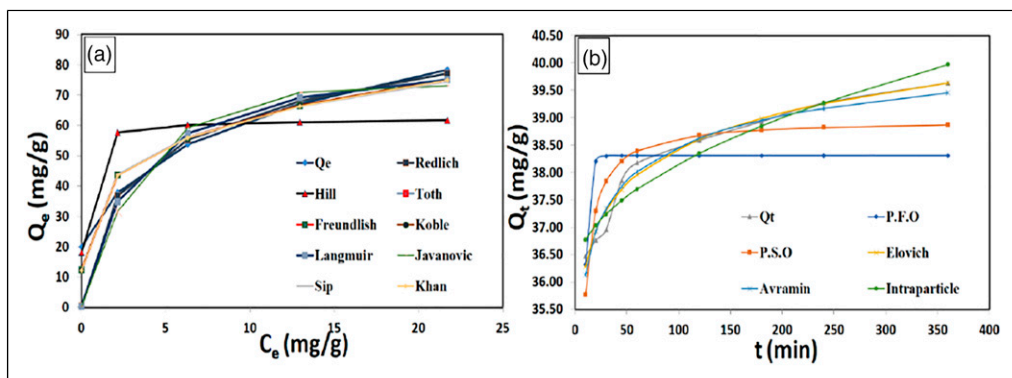
**Response surface methodology.** Table 7 describes the positive linear relations for DY 50 removal using nano bentonite. Positive linear relations of the independent variables “pH,” “dose,”

**Table 3.** Results of isotherm models after using nano bentonite for DY 50 removal.

Model	Constant	Unit	Nano bentonite	Model	Constant	Unit	Nano bentonite
Javanovic	MPSD		1.02	<b>Hill</b>	MPSD		0.3488
	Q <sub>m</sub>	mg/g	73.261		Q <sub>H</sub>	(mg/L)	63.000
	K <sub>j</sub>	L/g	0.261		n <sub>H</sub>		0.610
Langmuir	MPSD		0.986	<b>Redlich–Peterson</b>	MPSD		0.948
	Q <sub>0</sub>	mg/g	86.008		K <sub>r</sub>	(L/mg)	56.465
	b		0.316		B <sub>r</sub>	(l/mg)	0.272
Koble–Corrigan	MPSD		<b>0.1728</b>	<b>Sips</b>	g		0.714
	A	(L/mg)n(Lnmg <sup>l</sup> - n/mg)	36.346		MPSD		0.183
	B	(L/mg)n	0.000		Q <sub>s</sub>	(mg/g)	675.165
	D		0.235		K <sub>s</sub>	(L/mg)	0.000
Freundlich	MPSD		<b>0.1728</b>	<b>Khan</b>	MPSD		0.177
	K <sub>f</sub>	((mg/g) (mg/L) - l/n)	36.346		Q <sub>k</sub>	(mg/g)	4.027
	n		4.248		B <sub>k</sub>		11190
Toth	MPSD		0.9860		A <sub>k</sub>		0.764
	K <sub>t</sub>	(mg/g)	9.274				
	at	(L/mg)	3.161				
	t		9.274				

**Table 4.** Results of experimental and calculated  $Q_e$  (mg/g) for all nonlinear isotherm models after using nano bentonite for anionic DY 50 removal.

Exp. $Q_e$	Calc. Redlich $Q_e$	Calc. Hill $Q_e$	Calc. Sips $Q_e$	Calc. Khan $Q_e$	Calc. Toth $Q_e$	Calc. Koble $Q_e$	Calc. Javanovic $Q_e$	Calc. Freundlich $Q_e$	Calc. Langmuir $Q_e$
19.9	0.54	18.05	12.13	12.16	0.27	12.29	0.19	12.29	0.27
37.84	36.72	57.60	43.92	43.49	34.91	43.57	31.60	43.57	34.91
53.7	55.25	60.07	56.20	55.97	57.27	56.06	59.14	56.06	57.27
67.04	68.01	61.08	66.15	66.35	69.14	66.43	70.79	66.43	69.14
78.3	77.00	61.59	74.20	74.92	75.07	75.00	73.01	75.00	75.07

**Figure 7.** (a) Adsorption isotherm and (b) kinetic studies.**Table 5.** Results of kinetics model after using nano bentonite for DY 50 removal.

Models	P.F.O.	P.S.O.	Elovich	Avrami	Intraparticle					
<b>Constants</b>	$Q_e$	83.70	$Q_e$	89.38	$\alpha$	2364.8	$Q_e$	89.80	$K_{id}$	2.99
	$K_1$	0.15	$K_2$	0.00001	$\beta$	0.11	$K_{av}$	0.56	$C_i$	61.60
<b>MPSD</b>		0.01042		0.00222		0.00225	$n_{av}$	0.40		0.00522
								<b>0.00146</b>		

**Table 6.** Thermodynamic parameters for DY 50 removal on nano bentonite at different temperatures.

$\Delta H$	$\Delta S$	$\Delta G$ (KJ mol <sup>-1</sup> )					
(KJ mol <sup>-1</sup> )	(J mol <sup>-1</sup> K <sup>-1</sup> )	T= 20°C	T= 30°C	T= 40°C	T= 50°C	T= 60°C	T= 70°C
-33.7	-74.2	-6.93	-7.21	-7.35	-7.34	-7.47	-7.16

**Table 7.** RSM for DY 50 removal using linear regression analysis.

Variables entered/removed for DY 50 removal		
Variables entered	Temperature, time, pH, dose, and the all requested variables entered	
Method	Enter	
Model summary		
R	0.974	
R <sup>2</sup>	0.950	
Adjusted R <sup>2</sup>	0.942	
Std. error of the estimate	1.779	
ANOVA		
Significance	<b>0.000</b>	
F-statistics	<b>120.516</b>	
Coefficients		
	<b>Itl</b>	<b>Sig.</b>
(Constant)	45.92	0.000
pH	18.6	0.000
Dose (g/L)	10.6	0.000
Time (min)	4.96	0.000
Temperature (°C)	0.41	0.967
Concentration (mg/L)	10.441	0.000

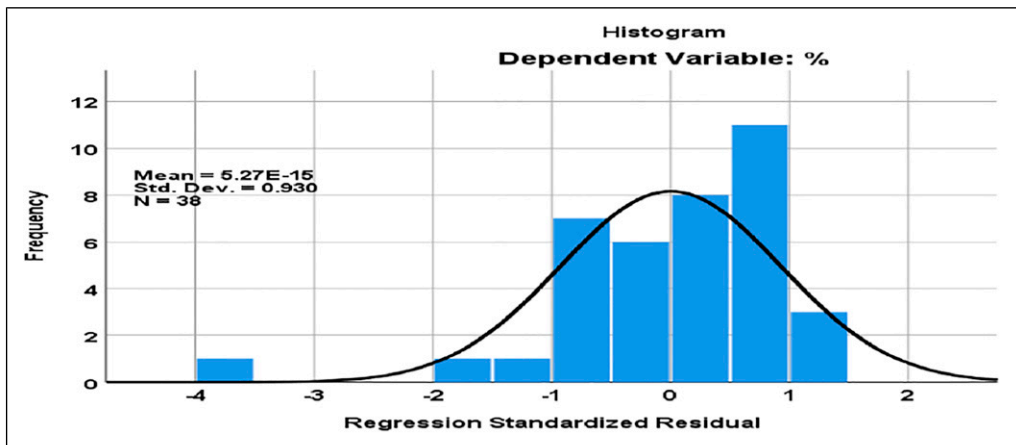


**Figure 8.** (a) Histogram for DY 50 removal using nano bentonite.

“time,” and “initial DY 50 concentration” were observed to be significant at  $p < 0.05$ . And, insignificant relation ( $p > 0.05$ ) for variable “temperature”. Figure 8 describes the histogram of DY 50 removal using nano bentonite, indicating that the frequency of the residual was between  $-1$  and  $1\%$ .

**Table 8.** ANNs for wastewater treatment after using nZVI by using multilayer perceptron.

Case processing summary		<b>N</b>	<b>Total</b>	<b>%</b>	<b>Valid</b>	<b>Excluded</b>
Sample	<b>Testing</b>	30	38	78.9%	100%	0%
	<b>Training</b>	8		21.1%		
Network information						
Input layer	Covariates	pH	Dose (g/L)	Time (min)	Temperature (°C)	Concentration (mg/L)
	Rescaling method for covariates				Standardized	
Hidden Layer(s)	Number of units in hidden layer excluding bias				6	
	Activation function				Hyperbolic tangent	
Output layer	Dependent variables	DY 50 removal %				
	Rescaling method for scale dependents			Standardized		
	Activation function			Identity		
	Error function			Sum of squares		
Model summary						
			<b>Training</b>		<b>Testing</b>	
Sum of squares error			0.062		0.0652	
Average overall relative error			0.004		0.088	
Stopping rule used						
Independent variable importance						
			<b>Importance</b>		<b>Normalized importance %</b>	
	pH	0.293			93.7	
	Dose (g/L)	0.313			100	
	Time (min)	0.160			51.0	
	Temperature °C	0.024			7.5	
	Concentration mg/L	0.210			67.2	

Stopping rule used: 1 consecutive step (s) with no decrease in error and the error computations are based on the testing sample



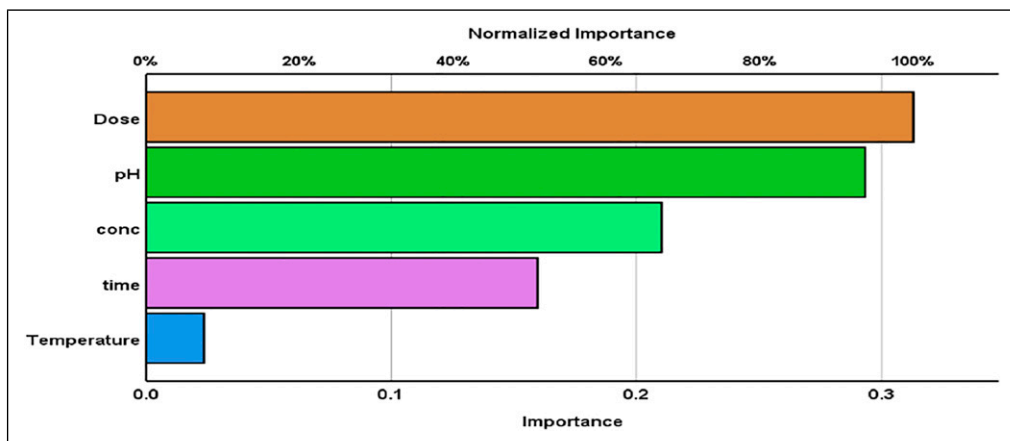


**Figure 9.** Importance and normalized importance for DY 50 removal using nano bentonite.

The coefficient of determination between measured data and simulated results ( $R^2$ ) and adjusted  $R^2$  existed in Table 7. By applying equation (7), the estimated removal equation is produced

$$Y_{(DY50)} = 99.037 - 3.055 x_1 + 12.283 x_2 + 0.023 x_3 - 0.001 x_4 - 0.247 x_5$$

where  $Y$  is the predicted response of removal efficiency (%);  $x_1$  is the pH (2–10);  $x_2$  is the adsorbent dose (0.2–1.8 g/L);  $x_3$  is the contact time (10–360 min);  $x_4$  is the temperature (20–70°C);  $x_5$  is the concentration (20–100 mg/L);  $\beta_0$  is the model intercept; and  $\beta_1$ ,  $\beta_2$ ,  $\beta_3$ ,  $\beta_4$ , and  $\beta_5$  are the linear coefficients of  $x_1$ ,  $x_2$ ,  $x_3$ ,  $x_4$ , and  $x_5$ , respectively.

*Artificial intelligence neural networks (ANNs).* Artificial intelligence neural networks were trained using the back-propagation algorithm for DY 50 removal by using nano bentonite. Network connects input layers via hidden layers and produces output layers. The network type, testing, training details, and other information are placed in Table 8.

The sample was trained 30 times and tested 8 times without excluding any result with a total number of 38 runs using network structure 5-3-1 as shown in Figure 1. The results indicated that the most significant operating parameter is the effect of dose 100% followed by the effect of pH 93.7% as shown in Figure 9 and Table 8. The ANN results indicated that there is a small deviation between the predictive and actual results as shown in Supplementary Figures 4 and 5. So, the residual percent between actual removal % and predicted removal % was between (−2.5, +2.5%). The obtained ANNs results agree with RSM, Kinetic, and thermodynamic results.

*Adsorption of DY 50 from aqueous solutions by various adsorbents.* Table 9 summarizes the removal efficiencies of direct yellow 50 using different sorbents (natural and synthesis). The result indicated that nano bentonite produces higher uptake at the lower time due to the

**Table 9.** Adsorption of DY 50 from aqueous solutions using various adsorbents.

Adsorbent	Experimental factor					DY 50 uptake (mg/g)	References
	pH	Adsorbent dosage, g/L	Contact time (min)	Initial concentration (mg/L)	Temperature (°C)		
Dimethyl diallyl ammonium chloride	4	1	80	30	25	14	76
Amberlite IRA 478, 958, 900, MP 68	Not sig.	NA	30	500	NA	50	60
<i>Mangifera indica</i> seed shell	2	1	120	50	35	34.62	82
Cotton fiber	7.03	33.3	120	113.3	25	28	83
Mesoporous activated carbon	7-9	1	Less than 120	10.65	NA	NA	84
Cotton	8	0.5 Cm <sup>2</sup>	NA	20	NA	NA	62
Titania-based adsorbent (Adsorbisia As500)	2	2	180	20	25	109.71	85
Rice straw	4	30 KGy	8 days	100	25	0.6	86
Starch/acrylonitrile-amidoxime	4	30 KGy	8 days	100	25	2.8	
Chemical-treated rice straw	4	30 KGy	8 days	100	25	2.8	
Nano bentonite	3	1	45	100	30	89	This study

NA: Not available.

chemisorption interaction between sorbed and adsorbed molecules and multi-layer adsorption behavior.

## Conclusions

This study showed that the nano bentonite was appropriate for the adsorption of DY 50 from aqueous solutions. The prepared nano bentonite was characterized using SEM, EDAX, XRD, XRF, TGA, and FT-IR indicating the formation of nano bentonite with an average size less than 50 nm. The effect of the operating parameter was conducted at different pH (2–10), dose (0.2–1.8 g/L), contact time from 10–360 min, at temperature 20–70°C, and initial DY 50 concentrations from 20–100 mg/L. The removal percentages were 100, 94.6, 89.5, 83.8, and 78.3% for initial concentration 20, 40, 60, 80, and 100 mg/L, respectively. The removal occurred at pH 2, using 1 g from nano bentonite, 45 min from contact time, and 30°C. Adsorption isotherm indicated that the adsorption mechanism was fitted to Freundlich and Koble–Corrigan models with the same lowest error sum of 0.1728 and showing a heterogeneous adsorption mechanism. Kinetic models indicated the adsorption process fitted to Pseudo-Second-Order. Thermodynamic behavior indicating that the adsorption behavior was exothermic with a spontaneous adsorption process. The RSM relations showing significant relations in removal models with a  $p$ -value  $<0.001$  and all operating variables are significant except effect of temperature. The ANN results indicated that the most effective operating conditions are the effect of dose followed by the pH effect.

## Declaration of conflicting interests

The author(s) declared no potential conflicts of interest with respect to the research, authorship, and/or publication of this article.

## Funding

The author(s) disclosed receipt of the following financial support for the research, authorship, and/or publication of this article: This study was supported by the Egyptian Housing and Building national Research Center (HBRC) and Nanotechnology Laboratory and Environmental services, Scientific Research Development unit (SRD), Egyptian Russian University (ERU).

## Supplemental Material

Supplemental material for this article is available online.

## References

1. Mahmoud AS, Farag RS, Elshfai MM, et al. Nano zero-valent aluminum (nZVAL) preparation, characterization, and application for the removal of soluble organic matter with artificial intelligence, isotherm study, and kinetic analysis. *Air Soil Water Res* 2019; 12: 1178622119878707.
2. El-Shafei M, Mahmoud AS, Mostafa M, et al. Effects of entrapped nZVI in alginate polymer on BTEX removal. In: *AIChE annual meeting*, San Francisco, CA, November 13-18, 2016.
3. Farag RS, Elshfai MM, Mahmoud AS, et al. *Green synthesis of nano iron carbide: preparation, characterization and application for aqueous phosphate removal*. In: *Aper presented at the environmental division 2018 - core programming area at the 2018 AIChE Annual Meeting*, 307–317, 2018. AIChE Annual Meeting October 28 - November 2, Lawrence Convention Center, Pittsburgh, PA

4. Mahmoud AS, Mostafa MK and Abdel-Gawad SA. Artificial intelligence for the removal of benzene, toluene, ethyl benzene and xylene (BTEX) from aqueous solutions using iron nanoparticles. *Water Supply* 2018; 18(5): 1650–1663.
5. Karam A, Zaher K and Mahmoud AS. Comparative studies of using nano zerovalent iron, activated carbon, and green synthesized nano zerovalent iron for textile wastewater color removal using artificial intelligence, regression analysis, adsorption isotherm, and kinetic studies. *Air Soil Water Res* 2020; 13: 1178622120908273.
6. Mahmoud AS, SaryEl-deen RA, Mostafa M, et al. Artificial intelligence for organochlorine pesticides removal from aqueous solutions using entrapped nZVI in alginate biopolymer. In: 2017 annual AIChE meeting, Minneapolis, MN, 29 October–3 November 2017.
7. Zhao F, Rahunen N, Varcoe JR, et al. Factors affecting the performance of microbial fuel cells for sulfur pollutants removal. *Biosens Bioelectron* 2009; 24(7): 1931–1936.
8. SaryEl-deen RA, Mahmoud AS, Mahmoud MS, et al. *Adsorption and kinetic studies of using entrapped sewage sludge ash in the removal of chemical oxygen demand from domestic wastewater, with artificial intelligence approach*. In: 2017 Annual AIChE meeting, 2017, October 29 - November 3, 2017 | Minneapolis Convention Center, Minneapolis, MN.
9. Walterick GC Jr. *Process for reducing color contamination of influent water*. Google Patents, 1987.
10. Pye K. Characteristics and significance of some humate-cemented sands (humicretes) at Cape Flattery, Queensland, Australia. *Geol Mag* 1982; 119(3): 229–242.
11. Satyawali Y and Balakrishnan M. Wastewater treatment in molasses-based alcohol distilleries for COD and color removal: a review. *J Environ Manage* 2008; 86(3): 481–497.
12. Antoniou MG, Nicolaou PA, Shoemaker JA, et al. Impact of the morphological properties of thin TiO<sub>2</sub> photocatalytic films on the detoxification of water contaminated with the cyanotoxin, microcystin-LR. *Appl Catal B: Environ* 2009; 91(1): 165–173.
13. Gao Y and Xia J. Chromium contamination accident in China: viewing environment policy of China. *Environ Sci Technol* 2011; 45(20): 8605–8606.
14. Kant R. *Textile dyeing industry an environmental hazard*, 2011.
15. Hao OJ, Kim H and Chiang PC. Decolorization of wastewater. *Crit Rev Environ Sci Technol* 2000; 30(4): 449–505.
16. Hunger K. *Industrial dyes: chemistry, properties, applications*. Hoboken: John Wiley & Sons, 2007.
17. Buxbaum G. *Industrial inorganic pigments*. Hoboken: John Wiley & Sons, 2008.
18. Correia VM, Stephenson T and Judd SJ. Characterisation of textile wastewaters—a review. *Environ Technol* 1994; 15(10): 917–929.
19. Bisschops I and Spanjers H. Literature review on textile wastewater characterisation. *Environ Technol* 2003; 24(11): 1399–1411.
20. Ryther JH and Dunstan WM. Nitrogen, phosphorus, and eutrophication in the coastal marine environment. *Science* 1971; 171(3975): 1008–1013.
21. Zahavi A. Mate selection—a selection for a handicap. *J Theor Biol* 1975; 53(1): 205–214.
22. Azbar N, Bayram A, Muezzinoglu A, et al. A review of waste management options in olive oil production. *Crit Rev Environ Sci Technol* 2004; 34(3): 209–247.
23. Lin SH and Peng CF. Treatment of textile wastewater by electrochemical method. *Water Res* 1994; 28(2): 277–282.
24. Georgiou D, Aivazidis A, Hatiras J, et al. Treatment of cotton textile wastewater using lime and ferrous sulfate. *Water Res* 2003; 37(9): 2248–2250.
25. Wawrzkievicz M and Polska-Adach E. Physicochemical interactions in systems CI Direct Yellow 50—Weakly basic resins: kinetic, equilibrium, and auxiliaries addition aspects. *Water* 2021; 13(3): 385.

26. Heberling JA, Mahmoud AS, Mostafa MK, et al. AOP performance at wastewater treatment plants. In: Proc. 2018 Annual AIChE Meeting, Pittsburgh, PA, 28 October–2 November 2018.
27. Mahmoud AS, Ismail A, Mostafa MK, et al. Isotherm and kinetic studies for heptachlor removal from aqueous solution using Fe/Cu nanoparticles, artificial intelligence, and regression analysis. *Separat Sci Technol* 2020; 55(4): 684–696.
28. Mostafa MK, Mahmoud AS, SaryEl-deen RA, et al. Application of entrapped nano zero valent iron into cellulose acetate membranes for domestic wastewater treatment. In: 2017 Annual AIChE meeting, Minneapolis, MN, 29 October 29–3 November 2017.
29. Farag RS, Mahmoud AS, Mostafa MK, et al. Study the degradation and adsorption processes of organic matters from domestic wastewater using chemically prepared and green synthesized nano zero-valent Iron. In: 2019 Annual AIChE meeting, Orlando, FL, 10–15 November, 2019. <https://www.researchgate.net/publication>
30. Elawwad A, Zaher K, Mahmoud AS, et al. Semi-Pilot plant for tertiary treatment of domestic wastewater using algal photo-bioreactor, with artificial intelligence. In: 2019 Annual AIChE meeting, Orlando, FL, 10–15 November, 2019. [https://www.researchgate.net/publication/337403206\\_562bb\\_Semi](https://www.researchgate.net/publication/337403206_562bb_Semi)
31. Verma AK, Dash RR and Bhunia P. A review on chemical coagulation/flocculation technologies for removal of colour from textile wastewaters. *J Environ Manage* 2012; 93(1): 154–168.
32. Ghernaout D, Ghernaout B and Kellil A. Natural organic matter removal and enhanced coagulation as a link between coagulation and electrocoagulation. *Desalination Water Treat* 2009; 2(1–3): 203–222.
33. Vandevivere PC, Bianchi R and Verstraete W. Treatment and reuse of wastewater from the textile wet-processing industry: review of emerging technologies. *J Chem Technol Biotechnol Int Res Process, Environ and Clean Technol* 1998; 72(4): 289–302.
34. Howard I, Espigares E, Lardelli P, et al. Evaluation of microbiological and physicochemical indicators for wastewater treatment. *Environ Toxicol An Int J* 2004; 19(3): 241–249.
35. Shon H, Vigneswaran S and Snyder SA. Effluent organic matter (EfOM) in wastewater: constituents, effects, and treatment. *Crit Rev Environ Sci Technol* 2006; 36(4): 327–374.
36. Rana MS, Sámano V, Ancheyta J, et al. A review of recent advances on process technologies for upgrading of heavy oils and residua. *Fuel* 2007; 86(9): 1216–1231.
37. Kadlec RH and Wallace S. *Treatment wetlands*. Boca Raton: CRC Press, 2008.
38. Renault F, Sancey B, Badot PM, et al. Chitosan for coagulation/flocculation processes—an eco-friendly approach. *Eur Polym J* 2009; 45(5): 1337–1348.
39. Grady CL Jr, Daigger GT, Love NG, et al. *Biological wastewater treatment*. Boca Raton: CRC Press, 2011.
40. Ariunbaatar J, Panico A, Esposito G, et al. Pretreatment methods to enhance anaerobic digestion of organic solid waste. *Appl Energy* 2014; 123: 143–156.
41. Fakhru'l-Razi A, Pendashteh A, Abdullah LC, et al. Review of technologies for oil and gas produced water treatment. *J Hazardous Mater* 2009; 170(2–3): 530–551.
42. Rupani PF, Singh RP, Ibrahim MH, et al. Review of current palm oil mill effluent (POME) treatment methods: vermicomposting as a sustainable practice. *World Appl Sci J* 2010; 11(1): 70–81.
43. Sauvignet P and Dahl CP. *Wastewater treatment method comprising decantation and fine screening stages*. Google Patents, 2011.
44. Naidoo S and Olaniran A. Treated wastewater effluent as a source of microbial pollution of surface water resources. *Int J Environ Res Public Health* 2014; 11(1): 249–270.
45. Graham TS. *Wastewater treatment system*, Google Patents, 1982.
46. Olsson G and Newell B. *Wastewater treatment systems*. London: IWA publishing, 1999.
47. Al-Rekabi WS, Qiang H and Qiang WW, Review on sequencing batch reactors. *Pak J Nutr* 2007; 6(1): 11–19.

48. Wu TY, Mohammad AW, Jahim JM, et al. Pollution control technologies for the treatment of palm oil mill effluent (POME) through end-of-pipe processes. *J Environ Manage* 2010; 91(7): 1467–1490.
49. Abdel-Raouf N, Al-Homaidan A and Ibraheem I. Microalgae and wastewater treatment. *Saudi J Biol Sci* 2012; 19(3): 257–275.
50. Cheremisinoff NP. *Handbook of water and wastewater treatment technologies*. Oxford: Butterworth-Heinemann, 2001.
51. Judd S. *The MBR book: principles and applications of membrane bioreactors for water and wastewater treatment*.: Elsevier, 2010.
52. Kollikkathara N, Feng H and Stern E. A purview of waste management evolution: special emphasis on USA. *Waste Manage*, 2009. 29(2): p. 974–985.
53. Farag RS, Mahmoud AS, Mostafa MK, et al. Green synthesis of nano iron carbide: preparation, characterization and application for removal of phosphate from aqueous solutions. In: Proc. 2018 Annual AIChE Meeting, Pittsburgh, PA, 28 October 28–2 November 2018.
54. Cincinelli A, Martellini T, Coppini E, et al. Nanotechnologies for removal of pharmaceuticals and personal care products from water and wastewater. a review. *J Nanosci Nanotechnol* 2015; 15(5): 3333–3347.
55. Ahmed MB, Zhou JL, Ngo HH, et al. Adsorptive removal of antibiotics from water and wastewater: progress and challenges. *Sci Total Environ* 2015; 532: 112–126.
56. Joshi M, Bansal R and Purwar R. *Colour removal from textile effluents*. India: NISCAIR-CSIR, 2004.
57. Mukhopadhyay R, Adhikari T, Sarkar B, et al. Fe-exchanged nano-bentonite outperforms Fe<sub>3</sub>O<sub>4</sub> nanoparticles in removing nitrate and bicarbonate from wastewater. *J Hazardous Mater* 2019; 376: 141–152.
58. Jana S, Ray J, Mondal B, et al. Efficient and selective removal of cationic organic dyes from their aqueous solutions by a nanocomposite hydrogel, katira gum-cl-poly (acrylic acid-co-N, N-dimethylacrylamide)@bentonite. *Appl Clay Sci* 2019; 173: 46–64.
59. Chinoune K, Bentaleb K, Boubberka Z, et al. Adsorption of reactive dyes from aqueous solution by dirty bentonite. *Appl Clay Sci* 2016; 123: 64–75.
60. Wawrzkiwicz M, Polska-Adach E and Hubicki Z. Polacrylic and polystyrene functionalized resins for direct dye removal from textile effluents. *Separat Sci Technol* 2020; 55(12): 2122–2136.
61. Abdel-Aziz HM, Farag RS and Abdel-Gawad SA. Carbamazepine removal from aqueous solution by green synthesis zero-valent iron/Cu nanoparticles with Ficus Benjamina leaves' extract. *Int J Environ Res* 2019; 13(5): 843–852.
62. Chrastil J. Adsorption of direct dyes on cotton: kinetics of dyeing from finite baths based on new information. *Textile Res J* 1990; 60(7): 413–416.
63. Mahmoud M and Mahmoud AS. Wastewater treatment using nano bimetallic iron/copper, adsorption isotherm, kinetic studies, and artificial intelligence neural networks. *Emergent Mater* 2021; 4: 1455–1463.
64. Mahmoud AS, Mohamed NY, Mostafa MK, et al. Effective chromium adsorption from aqueous solutions and tannery wastewater using bimetallic Fe/Cu nanoparticles: response surface methodology and artificial neural network. *Air Soil Water Res* 2021; 14: 11786221211028162.
65. Maha M, Elshfai ASM and Elsaid MA. Comparative studies of using nZVI and Entrapped nZVI in Alginate Biopolymer (Ag/ nZVI) for aqueous phosphate removal. In: 12th international conference on nano-technology for green and sustainable construction, 2021, Hurghada, Egypt. <https://www.researchgate.net/publication>
66. Mahmoud AS, Farag RS and Elshfai MM. Reduction of organic matter from municipal wastewater at low cost using green synthesis nano iron extracted from black tea: artificial intelligence with regression analysis. *Egypt J Pet* 2020; 29(1): 9–20.

67. Sadaf S, Bhatti HN, Nausheen S, et al. Application of a novel lignocellulosic biomaterial for the removal of Direct Yellow 50 dye from aqueous solution: batch and column study. *J Taiwan Inst Chem Eng* 2015; 47: 160–170.
68. Mittal A, Mittal J, Malviya A, et al. Decoloration treatment of a hazardous triarylmethane dye, Light Green SF (Yellowish) by waste material adsorbents. *J Colloid Interface Sci* 2010; 342(2): 518–527.
69. Darvishi Z and Morsali A. Synthesis and characterization of nano-bentonite by solvothermal method. *Colloids Surf A: Physicochem Eng Aspects* 2011; 377(1–3): 15–19.
70. Darvishi Z and Morsali A. Synthesis and characterization of Nano-bentonite by sonochemical method. *Ultrason Sonochem* 2011; 18(1): 238–242.
71. El-Nagar DA and Sary DH. Synthesis and characterization of nano bentonite and its effect on some properties of sandy soils. *Soil Tillage Res* 2021; 208: 104872.
72. Khatamian M, Divband B and Shahi R. Ultrasound assisted co-precipitation synthesis of Fe<sub>3</sub>O<sub>4</sub>/bentonite nanocomposite: performance for nitrate, BOD and COD water treatment. *J Water Process Eng* 2019; 31: 100870.
73. Dehgani Z, Sedghi asl M, Ghaedi M, et al. Removal of paraquat from aqueous solutions by a bentonite modified zero-valent iron adsorbent. *New J Chem* 2020; 44(31): 13368–13376.
74. Naghizadeh A and Gholami K. Bentonite and montmorillonite nanoparticles effectiveness in removal of fluoride from water solutions. *J Water Health* 2017; 15(4): 555–565.
75. Cozzolino D and Morón A. Potential of near-infrared reflectance spectroscopy and chemometrics to predict soil organic carbon fractions. *Soil Tillage Res* 2006; 85(1–2): 78–85.
76. Jabli M, Saleh TA, Sebeia N, et al. Dimethyl diallyl ammonium chloride and diallylamin Co-polymer modified bio-film derived from palm dates for the adsorption of dyes. *Scientific Rep* 2017; 7(1): 1–12.
77. Khodaer EA. Removal of direct 50 dyes from aqueous solution using natural clay and organoclay adsorbents. *Baghdad Sci J* 2015; 12(1): 157–166.
78. Diouri K, Chaqroune A, Kherbeche A, et al. Kinetics of Direct Yellow 50 dye adsorption onto marble powder sorbents. *Int J Innovative Res Sci Eng Technol* 2014; 3: 16626–16637.
79. Criado J and Ortega A. Non-isothermal crystallization kinetics of metal glasses: simultaneous determination of both the activation energy and the exponent n of the JMA kinetic law. *Acta Metallurgica* 1987; 35(7): 1715–1721.
80. Haq Iu, Bhatti HN and Asgher M. Removal of Solar Red BA textile dye from aqueous solution by low cost barley husk: equilibrium, kinetic and thermodynamic study. *Can J Chem Eng* 2011; 89(3): 593–600.
81. Ho YS, Chiang TH and Hsueh YM. Removal of basic dye from aqueous solution using tree fern as a biosorbent. *Process Biochem* 2005; 40(1): 119–124.
82. Jabeen A and Bhatti HN. Adsorptive removal of reactive green 5 (RG-5) and direct yellow 50 (DY-50) from simulated wastewater by *Mangifera indica* seed shell and its magnetic composite: Batch and Column study. *Environ Technol Innovation* 2021; 23: 101685.
83. Ismail L, Sallam HB, Abo Farha SA, et al. Adsorption behaviour of direct yellow 50 onto cotton fiber: equilibrium, kinetic and thermodynamic profile. *Spectrochimica Acta Part A: Mol Biomol Spectrosc* 2014; 131: 657–666.
84. Tamai H, Yoshida T, Sasaki M, et al. Dye adsorption on mesoporous activated carbon fiber obtained from pitch containing yttrium complex. *Carbon* 1999; 37(6): 983–989.
85. Wawrzkiwicz M, Polska-Adach E and Hubicki Z. Application of titania based adsorbent for removal of acid, reactive and direct dyes from textile effluents. *Adsorption* 2019; 25(3): 621–630.
86. Abdel-Aal S, Gad Y and Dessouki A. Use of rice straw and radiation-modified maize starch/acrylonitrile in the treatment of wastewater. *J Hazardous Mater* 2006; 129(1–3): 204–215.